First-principles calculations of monolayer hexagonal boron nitride: Possibility of superconductivity

Xiao-Tian Jin,[1,2] Xun-Wang Yan,[3] and Miao Gao[1,2,*]

[1]*Department of Microelectronics Science and Engineering, School of Physical Science and Technology, Ningbo University, Zhejiang 315211, China*

[2]*Laboratory of Clean Energy Storage and Conversion, Ningbo University, Zhejiang 315211, China*

[3]*College of Physics and Engineering, Qufu Normal University, Shandong 273165, China*

(Received 5 January 2020; revised manuscript received 7 April 2020; accepted 8 April 2020; published 27 April 2020)

Based on density-functional first-principles calculations and the Wannier interpolation technique, we have investigated the electron-phonon coupling (EPC) in hole-doped monolayer hexagonal boron nitride (h-BN). We align the Fermi level to a Van Hove singularity by 0.4 holes/cell doping, the largest hole concentration that can be realized in monolayer h-BN. Under this doping level, the EPC for free-standing monolayer h-BN is weak. However, biaxial tensile strain can enhance the EPC significantly. We predict that monolayer h-BN can become a phonon-mediated superconductor by the synergic effects of hole doping and biaxial tensile strain, with transition temperature exceeding 40 K.

DOI: 10.1103/PhysRevB.101.134518

I. INTRODUCTION

Inducing superconductivity in two-dimensional (2D) films, especially in graphene, has triggered a huge surge of research interest. Through the proximity effect, supercurrent was observed in graphene contacted by two closely spaced superconducting electrodes [1]. A mean-field phase diagram for superconductivity in graphene was derived by Uchoa and coworker. They suggested that the pairing interaction in metal coated graphene is likely mediated by a screened acoustic plasmon of the metal [2]. The EPC in graphene decorated by Li and Ca atoms was determined by density-functional first-principles calculations. It was predicted that the out-of-place carbon phonons become more active in monolayer than in the bulk phase, giving rise to phonon-mediated superconductivity in monolayer LiC_6 with the transition temperature T_c being 8.1 K [3]. Afterwards, the emergence of superconductivity at 7.4 K in Li-intercalated few-layer-graphene was confirmed [4]. The modulation of EPC in graphene under heavy electron/hole doping and biaxial tensile strain (BTS) was theoretically investigated. A high T_c of about 31.6 K was anticipated in hole-doped graphene with the BTS being 16.5% [5]. Recently, Cao *et al.* reported that bilayer graphene with a small twist angle of about 1.1° is in a correlated insulating state. Further applying electrostatic doping, superconductivity occurs at 1.7 K in bilayer graphene, which behaves in analogy with cuprates [6,7]. This discovery may shed light on understanding the unconventional mechanism of high-T_c superconductivity.

Hexagonal boron nitride (h-BN), the structural and isoelectric analog of graphite, is an insulator with a large energy gap of about 6 eV [8,9]. Due to its outstanding properties, h-BN has a wide range of applications, for example, as deep ultraviolet emitter [8,10], x-ray lithography mask [11], wear-resistant lubricant [12], dielectric layer [13], membrane for strong oxidation resistance [14], and inorganic filler [15]. Particularly, h-BN is an excellent supporting substrate for graphene nanodevices [16–18] because of its atomically smooth surface, free of dangling bonds, small lattice mismatch, and the ability to engineer the electronic structure of graphene. It was demonstrated that the mobilities and carrier inhomogeneities of graphene devices on h-BN substrates are nearly an order of magnitude better than those on SiO_2 substrates [16]. Monolayer h-BN, often referred as white graphene, can be prepared by chemical vapor deposition (CVD) of borazine ($B_3N_3H_6$) or borazane (H_3BNH_3) on metal foils [19–21]. Utilizing the weak van der Waals interaction between adjacent layers, exfoliation of h-BN is a feasible way to produce BN nanosheets, such as through micromechanical cleavage [22], functionalization using lipophilic and hydrophilic amine molecules [23], and sonication [24].

Due to the insulating nature, extra carriers must be added first to drive h-BN sheets into a potential superconducting state. Recently, Shimada *et al.* introduced electron doping in bilayer h-BN by Li intercalation. The computed EPC was suggested to bring about a T_c of 25 K for phonon-mediated superconductivity [25]. In sharp contrast with the weak EPC in Li-intercalated bilayer graphene, the formation of interlayer boron-boron bonds is crucial to enhance the EPC in Li-intercalated bilayer h-BN [25]. However, the strength of EPC in doped monolayer h-BN remains unclear. Very recently, Moriyama *et al.* constructed a h-BN/nontwisted bilayer graphene/h-BN Moiré superlattice, with a small angle near zero between one of the two h-BN sheets and the bilayer graphene [26]. A superconducting dome with the highest critical temperature of 14 K was observed upon *in situ* electrostatic doping [26]. This indicates that the interfacial interaction between h-BN sheets and bilayer graphene plays an essential role to pair electrons, and the twist angle

*gaomiao@nbu.edu.cn

in bilayer graphene is not necessary. Moreover, monolayer h-BN is always employed as a fundamental building block to fabricate 2D heterostructures [27], thus it is very interesting to know whether monolayer h-BN can become a high-T_c superconductor under specific modulation, like graphene [5].

In this work, we have systematically investigated the EPC and phonon-mediated superconductivity in hole-doped monolayer h-BN, based on density-functional first-principles calculations and Wannier interpolation. The Fermi level is adjusted to match a Van Hove singularity by 0.4 holes/cell doping. This is also the upper limit of hole concentration that can be accessed in monolayer h-BN. Significant imaginary phonon modes emerge under excess doping. We find that the EPC is quite weak in monolayer h-BN under 0.4 holes/cell doping, and no superconductivity transition occurs. But BTS can dramatically enhance the EPC resulting from softened phonon modes and enlarged density of states (DOS) at the Fermi level. Particularly, the EPC for hole-doped monolayer h-BN under the largest BTS is 2.75, about twice that of hole-doped graphene, leading to a superconducting T_c of 41.6 K. The structure of the superconducting energy gap is further determined by solving the anisotropic Eliashberg equations. We reveal that hole-doped monolayer h-BN under BTS is a single-gap s-wave high-T_c superconductor, with a slight anisotropy.

II. METHODS

In our calculations, the first-principles package QUANTUM-ESPRESSO was adopted [28]. A vacuum layer of 15 Å was inserted in the slab model to avoid the coupling between adjacent BN sheets along the c axis. Hole doping is simulated by removing a certain amount of electrons from the system and adding a compensating background of uniform negative charges. We calculated the electronic states and phonon perturbation potentials [29] by using the generalized gradient approximation (GGA) of Perdew-Burke-Ernzerhof formula [30] and the optimized norm-conserving Vanderbilt pseudopotentials [31]. After the convergence test, the kinetic-energy cutoff and the charge-density cutoff were chosen to be 80 and 320 Ry, respectively. The charge densities were calculated on an unshifted mesh of $48 \times 48 \times 1$ points in combination with a Methfessel-Paxton smearing [32] of 0.02 Ry. The dynamical matrices and the perturbation potentials were computed on a Γ-centered $12 \times 12 \times 1$ mesh, within the framework of density-functional perturbation theory [33].

We used four functions as initial guess to construct the maximally localized Wannier functions (MLWFs) [34,35] of monolayer h-BN. Among them, one is the p_z orbital of nitrogen, and the other three are σ-like states localized in the middle of boron-nitrogen bonds. After optimization, these MLWFs exhibit excellent localization in space. Specifically, the average spatial spread of these four MLWFs in strain-free monolayer h-BN is just about 0.71 Å^2. Fine electron ($480 \times 480 \times 1$) and phonon ($120 \times 120 \times 1$) grids were used to interpolate the EPC constant through the WANNIER90 and EPW codes [36,37]. The Dirac δ functions for electrons and phonons were smeared out by a Gaussian function with the widths of 20 and 0.5 meV, respectively.

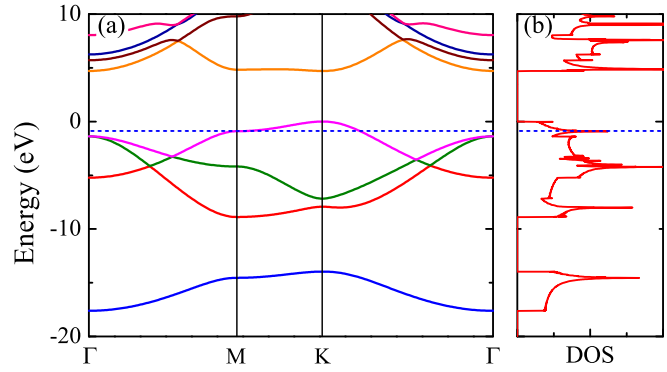

FIG. 1. Electronic structure for undoped monolayer h-BN: (a) band structure, (b) total DOS. The energy of the valance-band maximum is set to zero. The blue dashed line corresponds to a Van Hove singularity.

The isotropic Eliashberg spectral function $\alpha^2F(\omega)$ reads

$$\alpha^2F(\omega)=\frac{1}{\hbar N(0)N_{\mathbf{k}}N_{\mathbf{q}}}\sum_{\nu mn\mathbf{kq}}\left|g^{nm}_{\mathbf{k},\mathbf{q}\nu}\right|^2\delta\left(\epsilon^n_{\mathbf{k}}\right)\delta\left(\epsilon^m_{\mathbf{k}+\mathbf{q}}\right)\delta(\omega-\omega_{\mathbf{q}\nu}). \tag{1}$$

Here $N(0)$ is the DOS of electrons at the Fermi level. $N_{\mathbf{k}}$ and $N_{\mathbf{q}}$ represent the total numbers of $\mathbf{k}$ and $\mathbf{q}$ points in the fine $\mathbf{k}$ and $\mathbf{q}$ mesh. $g^{nm}_{\mathbf{k},\mathbf{q}\nu}$ is an EPC matrix element. (n, m) and ν denote the indices of energy bands and phonon mode, respectively. $\epsilon^n_{\mathbf{k}}$ and $\epsilon^m_{\mathbf{k}+\mathbf{q}}$ are the eigenvalues of the Kohn-Sham orbitals with respect to the Fermi level. $\omega_{\mathbf{q}\nu}$ is the phonon frequency. The EPC constant λ was determined by [38,39]

$$\lambda=\frac{1}{N_{\mathbf{q}}}\sum_{\mathbf{q}\nu}\lambda_{\mathbf{q}\nu}=2\int\frac{\alpha^2F(\omega)}{\omega}d\omega. \tag{2}$$

The coupling constant $\lambda_{\mathbf{q}\nu}$ measures the contribution to EPC from a given phonon mode $\mathbf{q}\nu$:

$$\lambda_{\mathbf{q}\nu}=\frac{2}{\hbar N(0)N_{\mathbf{k}}}\sum_{nm\mathbf{k}}\frac{1}{\omega_{\mathbf{q}\nu}}|g^{nm}_{\mathbf{k},\mathbf{q}\nu}|^2\delta\left(\epsilon^n_{\mathbf{k}}\right)\delta\left(\epsilon^m_{\mathbf{k}+\mathbf{q}}\right). \tag{3}$$

The superconducting transition temperature is determined by the McMillian-Allen-Dynes formula [39],

$$T_c=\frac{\omega_{\log}}{1.2}\exp\left[\frac{-1.04(1+\lambda)}{\lambda(1-0.62\mu^*)-\mu^*}\right], \tag{4}$$

in which μ^* is the Coulomb pseudopotential, and $\omega_{\log}$ is the logarithmic average frequency. When $\lambda \geqslant 1.3$, the correction to Eq. (4) was made accordingly [39].

III. RESULTS AND DISCUSSIONS

Figure 1 shows the band structure and total DOS for free-standing pristine monolayer h-BN. A direct energy band gap of about 4.7 eV can be found [Fig. 1(a)]. Close to the gap, there is a Van Hove singularity at −0.88 eV, as highlighted by the blue dashed line [Fig. 1(b)]. The reason to choose hole doping is that the valance band consists of bonding states, while the conduction band is contributed by antibonding states. Bonding states are more sensitive to lattice vibrations than the antibonding ones. Thus hole doping is

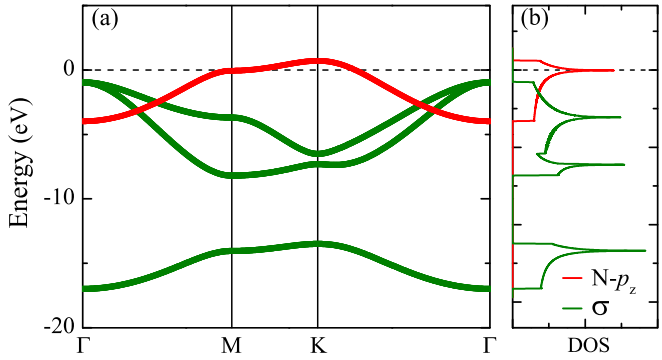

FIG. 2. Electronic structure for monolayer h-BN with 0.4 holes/cell doping: (a) band structure, (b) orbital-resolved density of states. The widths of the red and green lines represent the weights of N-p_z and sp^2-hybridized σ orbital at the given Bloch states, respectively. The Fermi level is set to zero. The empty energy bands are not shown.

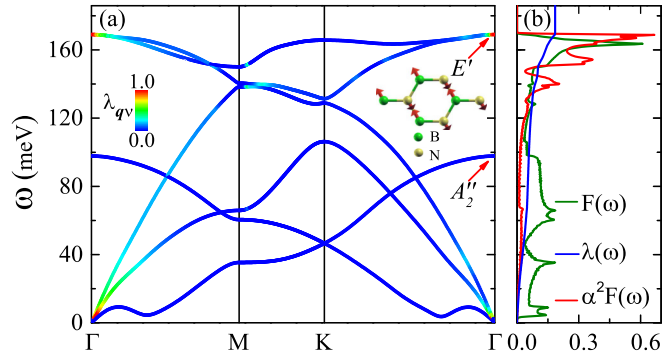

FIG. 3. Lattice dynamics of monolayer h-BN with 0.4 holes/cell doping: (a) phonon spectrum, with a color representation of $\lambda_{\mathbf{q}\nu}$. The phonon displacement for one of the E' modes is shown as the inset. (b) Phonon DOS $F(\omega)$, Eliashberg spectral function $\alpha^2F(\omega)$, and accumulated $\lambda(\omega)$. The accumulated $\lambda(\omega)$ is computed by using the formula $2\int_0^{\omega}\frac{1}{\omega'}\alpha^2F(\omega')d\omega'$. The graduation of $F(\omega)$ is omitted for clarity.

propitious to electron pairing. This is just the underlying physics in graphene, whereas the EPC of hole-doped graphene is always larger than in the electron-doped case [5]. Since superconductivity can benefit from a high DOS, we shift the Fermi level to approach the Van Hove singularity marked by the blue dashed line. As a result, about 0.4 electrons/cell should be removed from the system after integrating the DOS.

Figure 2 shows the band structure and projected DOS of monolayer h-BN under a doping level of 0.4 holes/cell. According to the orbital-resolved band structure, the partially occupied energy band is composed of N-p_z orbitals. As the valance-band maximum for undoped h-BN is at the K point [40], hole doping will result in a Fermi surface surrounding the K point [see Fig. 7(a)]. The other three bands are sp^2-hybridized σ-bonding bands. If the σ-bonding bands can cross the Fermi level, the EPC of monolayer h-BN will be promoted remarkably, as is the case for MgB_2 [41,42] and hole-doped LiBC [43,44]. We have tried to increase the doping concentration to 2.0 holes/cell; however, the N-p_z-associated band and the σ-bonding bands are gapped by 0.47 eV. As a consequence, N-p_z-associated band is totally empty, and the σ-bonding bands remain nonconductive.

Figure 3 shows the phonon spectrum, phonon DOS $F(\omega)$, Eliashberg spectral function $\alpha^2F(\omega)$, and accumulated $\lambda(\omega)$ for 0.4 holes/cell doped monolayer h-BN. All phonon modes have nonimaginary frequencies [Fig. 3(a)]. But the lowest acoustic-phonon mode near the Γ points has obvious softening. Further increasing the doping density to 0.5 holes/cell, we find that the softened modes become imaginary. The peak of $F(\omega)$ locates at 160 meV, owing to the weak dispersion of high-frequency optical modes [Fig. 3(b)]. The optical modes at the Γ point are identified to be E' and A_2'', respectively. The E' modes only involve the 2D in-plane movements of boron and nitrogen atoms [see the inset of Fig. 3(a)]. Near the Γ point, both E' modes and acoustic modes have strong coupling with electrons, indicating that the phonon linewidths for the E' modes are larger than that of the acoustic modes. The main peak of $\alpha^2F(\omega)$ surrounding 160 meV originates from two factors, i.e., the high-frequency strongly coupled E' modes and the structure of $F(\omega)$. The calculated EPC constant λ and $\omega_{\log}$ are 0.18 and 96.24 meV (see Table I), respectively. Such an EPC is too weak to pair electrons. As a result, free-standing monolayer h-BN is not superconducting.

Applying BTS to thin films is an effective method to raise T_c [5,45,46]. The reasons are twofold according to Eq. (3). First, BTS can weaken the atomic force constant, leading to softened phonon modes. Second, the overlap between atomic orbitals is reduced. The width of energy bands becomes narrower and the DOS at the Fermi level is enlarged. Based on this picture, we further investigate the modulation of EPC in monolayer h-BN versus BTS, defined by $\epsilon = (a - a_0)/a_0 \times 100\%$. Here a_0 and a are the in-plane lattice constants for free-standing ($a_0 = 2.507$ Å in our calculation) and strained cases, respectively. Figure 4 shows the phonon spectra under different BTS. The phonons exhibit gradual softening. Although there is a soft acoustic phonon mode in the equilibrium case [Fig. 3(a)], this mode does not become imaginary under the studied BTS. Interestingly, the frequency of the A_2'' mode at the Γ point is almost unaffected by BTS (see Table I and Fig. 4).

TABLE I. The calculated $N(0)$, frequencies of E' ($\omega_{E'}$) and A_2'' ($\omega_{A_2''}$) modes, EPC properties, and superconducting T_c for monolayer h-BN under BTS. $\omega_{\log}$ and $\langle\omega^2\rangle$ can be computed through $\exp[\frac{2}{\lambda}\int\frac{d\omega}{\omega}\alpha^2F(\omega)\ln\omega]$ and $\frac{2}{\lambda}\int d\omega\alpha^2F(\omega)\omega$. The T_c is determined with the McMillian-Allen-Dynes formula by setting μ_c^* to 0.1. The units for BTS, doping, $N(0)$, frequency, and T_c are %, holes/cell, states spin^{-1} eV^{-1} cell^{-1}, meV, and K, respectively.

ϵ	Doping	$N(0)$	$\omega_{E'}$	$\omega_{A_2''}$	$\omega_{\log}$	$\sqrt{\langle\omega^2\rangle}$	λ	T_c
0.0	0.4	0.50	169.03	97.80	96.24	128.89	0.18	0.0
5.0	0.4	0.58	136.97	99.12	69.62	99.69	0.26	0.1
10.0	0.4	0.68	109.29	97.48	51.67	74.20	0.40	2.4
15.0	0.4	0.79	84.55	93.53	27.29	44.42	0.94	19.9
16.0	0.4	0.81	79.87	92.50	20.91	36.52	1.35	28.0
17.0	0.4	0.84	75.26	91.40	11.54	25.04	2.77	33.4
17.5	0.4	0.85	73.46	90.58	14.90	24.98	2.75	41.6
17.5	0.5	1.01	76.42	90.44	19.94	30.78	1.88	38.6

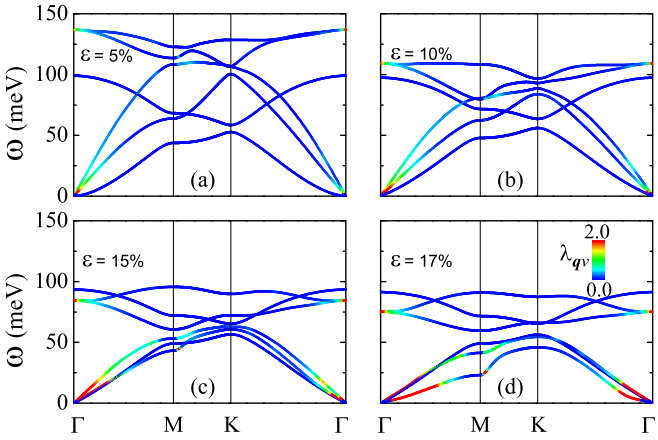

FIG. 4. Phonon spectra weighted by $\lambda_{\mathbf{q}\nu}$ under typical BTS.

Figure 5 shows the Eliashberg spectral functions in strained cases. As expected, the peaks of $\alpha^2F(\omega)$ are red shifted. And the low-frequency proportion becomes important. Especially for BTS = 17.5%, the largest BTS that can be imposed on monolayer h-BN, the EPC constant λ is dramatically enhanced to 2.75, about twice that of hole-doped graphene [5]. The superconducting T_c is calculated to be 41.6 K, also higher than hole-doped graphene and Li-intercalated bilayer h-BN. In comparison with 17%, the tiny decrease in λ for BTS of 17.5% still leads to a higher T_c. This is ascribed to the narrowed peak of $\alpha^2F(\omega)$ near 15 meV [Fig. 5], resulting in an amplified $\omega_{\log}$ (see Table I). The abnormal increase of $\alpha^2F(\omega)$ at about 108 meV under BTS of 10% can be attributed to the dispersionless behavior of A'' mode along the Γ-M and Γ-K lines [Fig. 4(b)]. This causes a very sharp $F(\omega)$ around 108 meV (Fig. 6). We must mention that undoped monolayer h-BN is unstable under 17.5% BTS (please see the Appendix for details).

It is known that the McMillian-Allen-Dynes formula underestimates T_c when the anisotropy of the Fermi surface is strong [46,47]. Therefore, we solve the anisotropic Eliashberg equations [47–49] self-consistently to examine the anisotropy of the Fermi surface and superconducting gaps. The

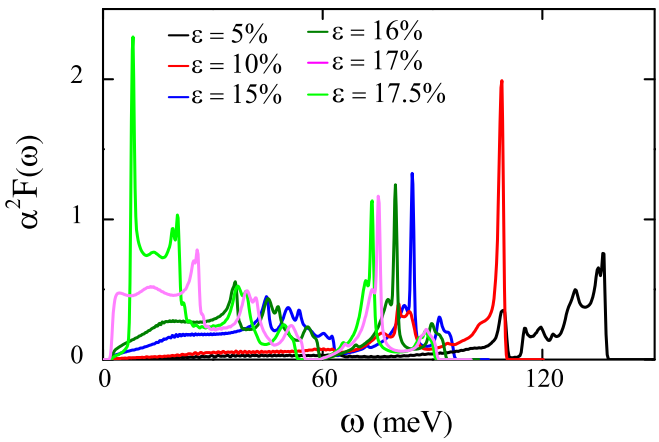

FIG. 5. Eliashberg spectral function $\alpha^2F(\omega)$ for 0.4 holes/cell-doped monolayer h-BN under various BTS.

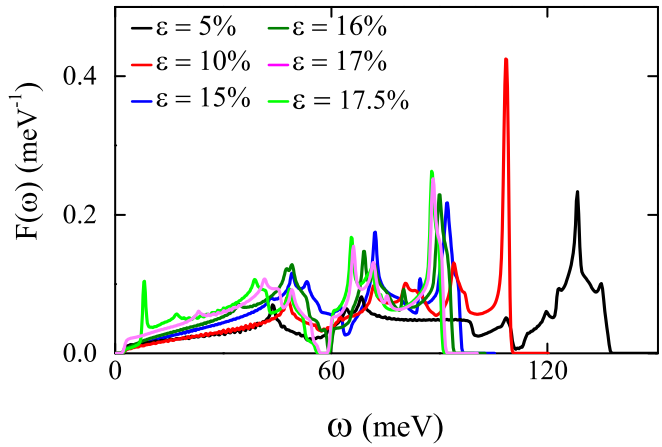

FIG. 6. Phonon density of states $F(\omega)$ for 0.4 holes/cell-doped monolayer h-BN under various BTS.

truncated frequency ω_c for the sum over Matsubara frequencies is selected as 1.0 eV, about 11 times that of the highest phonon frequency of 17.5%-strained monolayer h-BN. Two meshes, $360 \times 360 \times 1$ and $120 \times 120 \times 1$, are employed for electrons and phonons, respectively. Figure 7(a) shows the Fermi surface weighted by momentum-resolved EPC strength $\lambda_{n\mathbf{k}}$, suggesting that the Fermi-surface electronic states have a slightly anisotropic contribution to EPC. The distribution of the superconducting gap on the Fermi surface at 5 K is shown in Fig. 7(b). The symmetry is clearly s wave. From our calculation, the anisotropy ratio of the superconducting gap, Δ^{aniso}, defined by $(\Delta^{\max} - \Delta^{\min})/\Delta^{\text{ave}} = (10.68 - 8.34)/9.28 = 25.2\%$ [Fig. 7(d)]. This means that the anisotropy of the superconducting gap on the Fermi surface is not strong and confirms the validity of predicting T_c through the McMillian-Allen-Dynes formula. Compared with

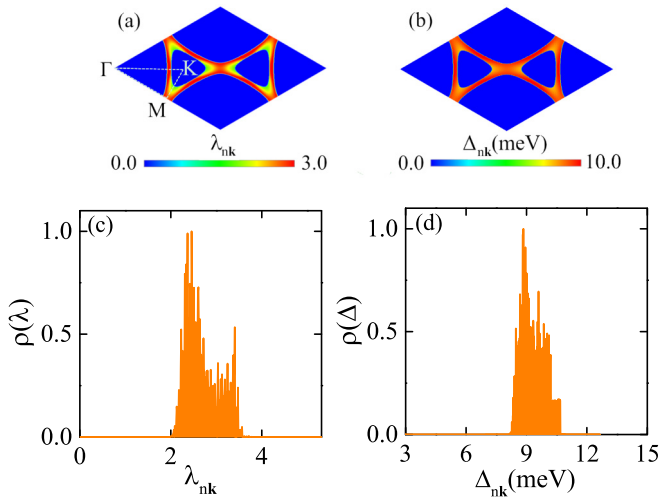

FIG. 7. (a) The momentum-resolved EPC strength $\lambda_{n\mathbf{k}}$ for each electronic state $n\mathbf{k}$ on the Fermi surface. $\lambda_{n\mathbf{k}}$ is computed through $\sum_{m\mathbf{k}'} \lambda(n\mathbf{k}, m\mathbf{k}', 0)\delta(\epsilon_{m\mathbf{k}'})/N(0)$ [48]. (b) Distribution of the superconducting gap $\Delta_{n\mathbf{k}}$ on the Fermi surface at 5 K. For convenience, these two figures were drawn in the reciprocal unit cell. (c) Normalized density of $\lambda_{n\mathbf{k}}$. (d) Normalized density of $\Delta_{n\mathbf{k}}$.

the multi-orbital superconductivity of MgB_2 [47,48], the weak anisotropy can be attributed to the fact that the Fermi-surface states are mostly from a single orbital, i.e., N-p_z.

IV. DISCUSSION

To realize the highest T_c of monolayer h-BN, a rather large charge density (n_{2D}) of 5.3×10^{14} cm^{-2} is needed. In recent years, electric double-layer transistors (EDLTs) have been widely employed for attaining ultrahigh-density carrier accumulation, with polymer electrolytes or ionic liquids being the gate dielectrics [50–56]. The liquid electrolyte forms an electric double layer at the solid-liquid interface, with typical thickness of 0.3–0.5 nm. Due to the ultrathin layer, extremely high capacitance and charge-carrier density can be achieved at the liquid-solid interface. Based on this technique, gate-induced superconductivity has been observed in $SrTiO_3$ [57–59], $KTaO_3$ [60], quasi-2D layered ZrNCl [61], transition-metal dichalcogenides [62–64], and cuprates [65–67]. Utilizing a ZnO field-effect transistor gated by electric double layers of the ionic liquid DEME-TFSI, it was found that the charge accumulation can reach an ultrahigh carrier density of 8×10^{14} cm^{-2} at 220 K and maintain a density of 5.5×10^{14} cm^{-2} at 1.8 K [68]. By using a novel polymer electrolyte solution, n_{2D} as high as 3.5×10^{15} cm^{-2} can be injected into gold films to induce large relative variations in the film resistance [69]. Hence, the reported n_{2D} can indeed satisfy the condition required by high-T_c monolayer h-BN. Besides liquid gating, solid-electrolyte gating is another promising method. For example, lithium-ion-based solid electrolytes can be used to modulate the electronic properties of ferromagnetic oxide thin film [70], graphene [71], and FeSe thin flakes [72]. Recently, Zhao *et al.* explored the performance of sodium-ion-based solid electrolyte and found that n_{2D} can reach a hole density of 3.0×10^{14} cm^{-2} and an electron density of 5.0×10^{14} cm^{-2} [73], comparable to these obtained through liquid gating.

Since the doping concentration of 0.4 holes/cell is quite high, we also examine the stability of 0.4 holes/cell-doped monolayer h-BN against vacancy-type defects. In the calculation, we adopt a 4×4 supercell, meanwhile keeping the same doping density as in the 1×1 cell. The atomic positions are fully relaxed to minimize the total energy after removing one boron or one nitrogen atom. Combined with the energies for α-B_{12} and molecular nitrogen, we find that the disadvantage in energy for a boron (nitrogen) vacancy is equal to 11.1 eV (4.6 eV). This suggests that the emergence of a vacancy-type defect is unfavorable.

It is noteworthy that the highest doping level constrained by the condition of dynamical stability in strain-free monolayer h-BN is 0.4 holes/cell. However, this critical value may vary in the strained case. For example, the phonons exhibit obvious hardening when we increase the doping concentration from 0.4 to 0.5 holes/cell for 17.5%-strained monolayer h-BN. Consequently, the imaginary phonon frequencies disappear. This means that monolayer h-BN is stable under 0.5 holes/cell doping and BTS of 17.5%. But the hardened phonons slightly suppress the superconductivity, with T_c reduced by 3 K (see Table I).

V. CONCLUSION

In summary, we present the first-principles calculations of electronic structure and EPC in monolayer h-BN under hole doping and BTS. The EPC strength is accurately determined based on the state-of-the-art Wannier interpolation technique. Since the T_c for conventional superconductors strongly relies on the DOS at the Fermi level, we adjust the Fermi level to match a Van Hove singularity through 0.4 holes/cell doping. This is also the largest hole density that can be afforded by monolayer h-BN. However, the EPC is too weak to make electron pairing in free-standing monolayer h-BN. We further find that applying BTS can raise the T_c significantly, with the highest T_c being about 41.6 K. This effect can be rationalized in terms of softened phonon modes and enlarged DOS at the Fermi level. Through solving the anisotropic Eliashberg equations, we reveal that the superconducting gap is of *s*-wave symmetry, with a slight anisotropy. Our solid calculations prove theoretically that a well-known insulator monolayer h-BN can become a high-T_c superconductor via electron-phonon mechanism. Our findings are important for constructing nanosuperconducting devices, as monolayer h-BN is a vital constituent part of heterostructures.

ACKNOWLEDGMENTS

This work was supported by the National Natural Science Foundation of China (Grants No. 11974194 and No. 11974207), and Zhejiang Provincial Natural Science Foundation of China (Grant No. LY17A040005). M.G. was also sponsored by K. C. Wong Magna Fund in Ningbo University.

APPENDIX: THE STABILITY OF MONOLAYER h-BN WITH BTS BEING 17.5%

From our calculations, undoped monolayer h-BN cannot afford BTS of 17.5%, since the phonon spectrum is unstable

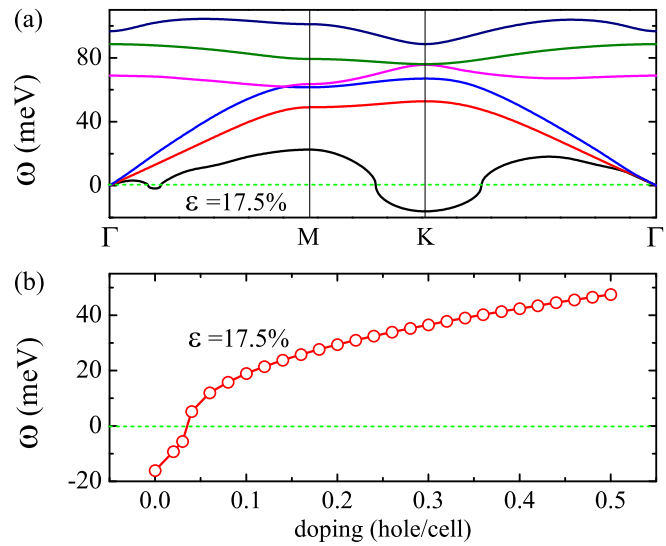

FIG. 8. (a) Phonon spectrum for undoped monolayer h-BN under BTS of 17.5%. (b) Frequency of the lowest acoustic *K*-point phonon under different doping concentration.

[Fig. 8(a)]. The largest imaginary phonon frequency is at the K point. But this mode is obviously hardened upon the increase of the hole-doping density. When the doping density is greater than 0.04 holes/cell, the imaginary mode at the K point disappears [Fig. 8(b)]. Thus hole-doped h-BN can be stable against BTS of 17.5%.

[1] H. B. Heersche, P. Jarillo-Herrero, J. B. Oostinga, L. M. K. Vandersypen, and A. F. Morpurgo, Nature (London) **446**, 56 (2007).

[2] B. Uchoa and A. H. Castro Neto, Phys. Rev. Lett. **98**, 146801 (2007).

[3] G. Profeta, M. Calandra, and F. Mauri, Nat. Phys. **8**, 131 (2012).

[4] A. P. Tiwari, S. Shin, E. Hwang, S.-G. Jung, T. Park, and H. Lee, arXiv:1508.06360.

[5] C. Si, Z. Liu, W. Duan, and F. Liu, Phys. Rev. Lett. **111**, 196802 (2013).

[6] Y. Cao, V. Fatemi, S. Fang, K. Watanabe, T. Taniguchi, E. Kaxiras, and P. Jarillo-Herrero, Nature (London) **556**, 43 (2018).

[7] Y. Cao, V. Fatemi, A. Demir, S. Fang, S. L. Tomarken, J. Y. Luo, J. D. Sanchez-Yamagishi, K. Watanabe, T. Taniguchi, E. Kaxiras, R. C. Ashoori, and P. Jarillo-Herrero, Nature (London) **556**, 80 (2018).

[8] Y. Kubota, K. Watanabe, O. Tsuda, and T. Taniguchi, Science **317**, 932 (2007).

[9] G. Cassabois, P. Valvin, and B. Gil, Nat. Photonics **10**, 262 (2016).

[10] K. Watanabe, T. Taniguchi, and H. Kanda, Nat. Mater. **3**, 404 (2004).

[11] S. S. Dana, Mater. Sci. Forum **54-55**, 229 (1991).

[12] K. Miyoshi, D. H. Buckley, J. J. Pouch, S. A. Alterovitz, and H. E. Sliney, Surf. Coat. Technol. **33**, 221 (1987).

[13] T. Sugino and T. Tai, Jpn. J. Appl. Phys. (1962–1981) **39**, L1101 (2000).

[14] L. H. Li, J. Cervenka, K. Watanabe, T. Taniguchi, and Y. Chen, ACS Nano **8**, 1457 (2014).

[15] T. H. Chiang and T.-E. Hsieh, J. Inorg. Organomet. Polym. Mater. **16**, 175 (2006).

[16] C. R. Dean, A. F. Young, I. Meric, C. Lee, L. Wang, S. Sorgenfrei, K. Watanabe, T. Taniguchi, P. Kim, K. L. Shepard, and J. Hone, Nat. Nanotechnol. **5**, 722 (2010).

[17] J. Xue, J. Sanchez-Yamagishi, D. Bulmash, P. Jacquod, A. Deshpande, K. Watanabe, T. Taniguchi, P. Jarillo-Herrero, and B. J. LeRoy, Nat. Mater. **10**, 282 (2011).

[18] W. Yang, G. Chen, Z. Shi, C.-C. Liu, L. Zhang, G. Xie, M. Cheng, D. Wang, R. Yang, D. Shi, K. Watanabe, T. Taniguchi, Y. Yao, Y. Zhang, and G. Zhang, Nat. Mater. **12**, 792 (2013).

[19] P. Sutter, J. Lahiri, P. Albrecht, and E. Sutter, ACS Nano **5**, 7303 (2011).

[20] K. K. Kim, A. Hsu, X. Jia, S. M. Kim, Y. Shi, M. Hofmann, D. Nezich, J. F. Rodriguez-Nieva, M. Dresselhaus, T. Palacios, and J. Kong, Nano Lett. **12**, 161 (2012).

[21] J.-H. Park, J. C. Park, S. J. Yun, H. Kim, D. H. Luong, S. M. Kim, S. H. Choi, W. Yang, J. Kong, K. K. Kim, and Y. H. Lee, ACS Nano **8**, 8520 (2014).

[22] D. Pacilé, J. C. Meyer, Ç. Ö. Girit, and A. Zettl, Appl. Phys. Lett. **92**, 133107 (2008).

[23] Y. Lin, T. V. Williams, and J. W. Connell, J. Phys. Chem. Lett. **1**, 277 (2010).

[24] W.-Q. Han, L. Wu, Y. Zhu, K. Watanabe, and T. Taniguchi, Appl. Phys. Lett. **93**, 223103 (2008).

[25] N. H. Shimada, E. Minamitani, and S. Watanabe, Appl. Phys. Express **10**, 093101 (2017).

[26] S. Moriyama, Y. Morita, K. Komatsu, K. Endo, T. Iwasaki, S. Nakaharai, Y. Noguchi, Y. Wakayama, E. Watanabe, D. Tsuya, K. Watanabe, and T. Taniguchi, arXiv:1901.09356.

[27] A. K. Geim and I. V. Grigorieva, Nature (London) **499**, 419 (2013).

[28] P. Giannozzi, S. Baroni, N. Bonini, M. Calandra, R. Car, C. Cavazzoni, D. Ceresoli, G. L. Chiarotti, M. Cococcioni, I. Dabo *et al.*, J. Phys.: Condens. Matter **21**, 395502 (2009).

[29] F. Giustino, M. L. Cohen, and S. G. Louie, Phys. Rev. B **76**, 165108 (2007).

[30] J. P. Perdew, K. Burke, and M. Ernzerhof, Phys. Rev. Lett. **77**, 3865 (1996).

[31] D. R. Hamann, Phys. Rev. B **88**, 085117 (2013).

[32] M. Methfessel and A. T. Paxton, Phys. Rev. B **40**, 3616 (1989).

[33] S. Baroni, S. de Gironcoli, A. Dal Corso, and P. Giannozzi, Rev. Mod. Phys. **73**, 515 (2001).

[34] N. Marzari and D. Vanderbilt, Phys. Rev. B **56**, 12847 (1997).

[35] I. Souza, N. Marzari, and D. Vanderbilt, Phys. Rev. B **65**, 035109 (2001).

[36] A. A. Mostofi, J. R. Yates, Y.-S. Lee, I. Souza, D. Vanderbilt, and N. Marzari, Comput. Phys. Commun. **178**, 685 (2008).

[37] J. Noffsinger, F. Giustino, B. D. Malone, C.-H. Park, S. G. Louie, and M. L. Cohen, Comput. Phys. Commun. **181**, 2140 (2010).

[38] P. B. Allen, Phys. Rev. B **6**, 2577 (1972).

[39] P. B. Allen and R. C. Dynes, Phys. Rev. B **12**, 905 (1975).

[40] X. Blase, A. Rubio, S. G. Louie, and M. L. Cohen, Europhys. Lett. **28**, 335 (1994).

[41] J. M. An and W. E. Pickett, Phys. Rev. Lett. **86**, 4366 (2001).

[42] Y. Kong, O. V. Dolgov, O. Jepsen, and O. K. Andersen, Phys. Rev. B **64**, 020501(R) (2001).

[43] H. Rosner, A. Kitaigorodsky, and W. E. Pickett, Phys. Rev. Lett. **88**, 127001 (2002).

[44] M. Gao, Z.-Y. Lu, and T. Xiang, Phys. Rev. B **91**, 045132 (2015).

[45] A. V. Pogrebnyakov, J. M. Redwing, S. Raghavan, V. Vaithyanathan, D. G. Schlom, S. Y. Xu, Qi Li, D. A. Tenne, A. Soukiassian, X. X. Xi, M. D. Johannes, D. Kasinathan, W. E. Pickett, J. S. Wu, and J. C. H. Spence, Phys. Rev. Lett. **93**, 147006 (2004).

[46] M. Gao, X.-W. Yan, Z.-Y. Lu, and T. Xiang, Phys. Rev. B **101**, 094501 (2020).

[47] H. J. Choi, D. Roundy, H. Sun, M. L. Cohen, and S. G. Louie, Nature (London) **418**, 758 (2002).

[48] E. R. Margine and F. Giustino, Phys. Rev. B **87**, 024505 (2013).

[49] E. R. Margine and F. Giustino, Phys. Rev. B **90**, 014518 (2014).

[50] H. Shimotani, G. Diguet, and Y. Iwasa, Appl. Phys. Lett. **86**, 022104 (2005).
[51] M. J. Panzer and C. D. Frisbie, J. Am. Chem. Soc. **127**, 6960 (2005).
[52] M. J. Panzer and C. D. Frisbie, Adv. Funct. Mater. **16**, 1051 (2006).
[53] J. Takeya, K. Yamada, K. Hara, K. Shigeto, K. Tsukagoshi, S. Ikehata, and Y. Aoyagi, Appl. Phys. Lett. **88**, 112102 (2006).
[54] H. Shimotani, H. Asanuma, and Y. Iwasa, Jpn. J. Appl. Phys. (1962–1981) **46**, 3613 (2007).
[55] L. Herlogsson, X. Crispin, N. D. Robinson, M. Sandberg, O.-J. Hagel, G. Gustafsson, and M. Berggren, Adv. Mater. **19**, 97 (2007).
[56] R. Misra, M. McCarthy, and A. F. Hebard, Appl. Phys. Lett. **90**, 052905 (2007).
[57] K. Ueno, S. Nakamura, H. Shimotani, A. Ohtomo, N. Kimura, T. Nojima, H. Aoki, Y. Iwasa, and M. Kawasaki, Nat. Mater. **7**, 855 (2008).
[58] Y. Lee, C. Clement, J. Hellerstedt, J. Kinney, L. Kinnischtzke, X. Leng, S. D. Snyder, and A. M. Goldman, Phys. Rev. Lett. **106**, 136809 (2011).
[59] P. Gallagher, M. Lee, J. R. Williams, and D. Goldhaber-Gordon, Nat. Phys. **10**, 748 (2014).
[60] K. Ueno, S. Nakamura, H. Shimotani, H. T. Yuan, N. Kimura, T. Nojima, H. Aoki, Y. Iwasa, and M. Kawasaki, Nat. Nanotechnol. **6**, 408 (2011).
[61] J. T. Ye, S. Inoue, K. Kobayashi, Y. Kasahara, H. T. Yuan, H. Shimotani, and Y. Iwasa, Nat. Mater. **9**, 125 (2010).
[62] J. T. Ye, Y. J. Zhang, R. Akashi, M. S. Bahramy, R. Arita, and Y. Iwasa, Science **338**, 1193 (2012).
[63] S. Jo, D. Costanzo, H. Berger, and A. F. Morpurgo, Nano Lett. **15**, 1197 (2015).
[64] W. Shi, J. Ye, Y. Zhang, R. Suzuki, M. Yoshida, J. Miyazaki, N. Inoue, Y. Saito, and Y. Iwasa, Sci. Rep. **5**, 12534 (2015).
[65] A. T. Bollinger, G. Dubuis, J. Yoon, D. Pavuna, J. Misewich, and I. Božović, Nature (London) **472**, 458 (2011).
[66] X. Leng, J. Garcia-Barriocanal, S. Bose, Y. Lee, and A. M. Goldman, Phys. Rev. Lett. **107**, 027001 (2011).
[67] S. W. Zeng, Z. Huang, W. M. Lv, N. N. Bao, K. Gopinadhan, L. K. Jian, T. S. Herng, Z. Q. Liu, Y. L. Zhao, C. J. Li *et al.*, Phys. Rev. B **92**, 020503(R) (2015).
[68] H. Yuan, H. Shimotani, A. Tsukazaki, A. Ohtomo, M. Kawasaki, and Y. Iwasa, Adv. Funct. Mater. **19**, 1046 (2009).
[69] D. Daghero, F. Paolucci, A. Sola, M. Tortello, G. A. Ummarino, M. Agosto, R. S. Gonnelli, J. R. Nair, and C. Gerbaldi, Phys. Rev. Lett. **108**, 066807 (2012).
[70] T. Tsuchiya, K. Terabe, M. Ochi, T. Higuchi, M. Osada, Y. Yamashita, S. Ueda, and M. Aono, ACS Nano **10**, 1655 (2016).
[71] J. Zhao, M. Wang, H. Li, X. Zhang, L. You, S. Qiao, B. Gao, X. Xie, and M. Jiang, Sci. Rep. **6**, 34816 (2016).
[72] B. Lei, N. Z. Wang, C. Shang, F. B. Meng, L. K. Ma, X. G. Luo, T. Wu, Z. Sun, Y. Wang, Z. Jiang, B. H. Mao, Z. Liu, Y. J. Yu, Y. B. Zhang, and X. H. Chen, Phys. Rev. B **95**, 020503(R) (2017).
[73] J. Zhao, M. Wang, X. Zhang, Y. Lv, T. Wu, S. Qiao, S. Song, and B. Gao, Sci. Rep. **7**, 3168 (2017).